

Article

# Characterization of Diatomaceous Earth and Halloysite Resources of Poland

Marcin Lutyński <sup>1,\*</sup> , Piotr Sakiewicz <sup>2</sup> and Sylwia Lutyńska <sup>3</sup>

<sup>1</sup> Department of Mining, Faculty of Mining, Safety Engineering and Industrial Automation, Silesian University of Technology, ul. Akademicka 2, 44-100 Gliwice, Poland

<sup>2</sup> Division of Nanocrystalline and Functional Materials and Sustainable Proecological Technologies, Institute of Engineering Materials and Biomaterials, Faculty of Mechanical Engineering, Silesian University of Technology, Konarskiego 18a, 44-100 Gliwice, Poland; piotr.sakiewicz@polsl.pl

<sup>3</sup> Department of Applied Geology, Faculty of Mining, Safety Engineering and Industrial Automation, Silesian University of Technology, ul. Akademicka 2, 44-100 Gliwice, Poland; sylwia.lutynska@polsl.pl

\* Correspondence: marcin.lutyński@polsl.pl

Received: 28 August 2019; Accepted: 29 October 2019; Published: 31 October 2019



**Abstract:** The mining industry of Poland is based mostly on coal and copper ores. Strict carbon emissions and the depletion of deposits will slowly phase out coal. Therefore, metallic ores and other mineral raw materials will dominate the extractive industry of Poland. Current measured resources of the largest deposits of halloysite and diatomaceous earth in Poland are over 0.5 Mt and 10 Mt, respectively. Halloysite and diatomaceous earth samples from halloysite Dunino deposits and Jawornik diatomaceous earth deposits (composed mostly of diatomaceous skeletons (frustules)) were subjected to mineralogical analysis, scanning electron microscopy/energy-dispersive X-ray spectroscopy (SEM-EDS) nanostructural, chemical, elemental, and mineral content analysis. Both these minerals have similar properties, i.e., sorption capacity and cation exchange capacity, and are used mostly for the same purposes, e.g., adsorbents, filler material, and filtration. Samples of Dunino halloysite consist of minerals such as halloysite, kaolinite, hematite, magnetite, quartz, magnesioferrite, rutile, ilmenite, geikielite, goyazite, gorceixite, and crandallite, with little impurities in the form of iron oxides. Occasionally, halloysite nanoplates (HNP) nanotubes (HNT) were found. Diatomaceous earth is composed mainly of silica-containing phases (quartz, opal) and clay minerals (illite and kaolinite). The frustules of diatoms are mostly centric (discoïd) and have radius values of approximately 50–60 µm. Large resources of these minerals could be used in the future either for manufacturing composite materials or highly advanced adsorbents.

**Keywords:** halloysite; diatomite; mineral deposit; mineral absorbent

## 1. Introduction

Central Europe has abundant resources of numerous deposits that include metallic ores and fossil fuels [1]. The mining of metallic ores started in the period of the Roman Empire, and advances in mining and processing technology allowed for extensive exploration in the 10th century AD [2]. Most of the easily accessible deposits were already exhausted in the 14th century, yet mining was revived in central Europe in the mid-15th century. This was caused by the increased demand for new kinds of metal ores (e.g., copper), technological innovations such as water pumping from shafts, and hydrometallurgical methods of metal separation [3]. In the 18th century, the Industrial Revolution brought interest in coal mining, and regions such as Ruhr in Germany and Silesia in Poland were the ones in Central Europe where the coal industry played a major role in the development of new mining technologies. Today, Poland still remains a major coal producer in the European Union with over

61.436 Gt of hard coal resources, out of which 3.605 Gt are proven reserves. Other important industrial minerals of Poland include metallic ores, which are mostly copper with recoverable reserves of 1.188 Gt. It is worth mentioning that other valuable minerals such as gold, silver, and nickel are extracted from copper ores. In 2018, 1.189 Mt of silver, 523 kg of gold, 1.73 Mt of nickel sulfate, and 66.35 t of selenium were recovered by KGHM Polska Miedź S.A., making a Polish company one of the world's largest silver producers [4]. Taking into account current production figures of the most important industrial minerals, we can assume that coal reserves will last for the next 20–30 years, whereas copper ore reserves should suffice for the next 50 years. Taking carbon emission limits into consideration, the coal mining industry will be phasing out in the next 10–15 years. Therefore, metallic ores and other mineral raw materials (except fossil fuels) will dominate the extractive industry of Poland.

Other industrial minerals of Poland include chemical raw materials such as barite and fluorspar, clay raw materials for the production of mineral paints, diatomaceous rock, potassium, and magnesium salts, but also siliceous earth and native sulfur [4].

The purpose of this study is a quantitative and qualitative evaluation of two industrial minerals used as effective adsorbents i.e., halloysite and diatomite (diatomaceous earth). These minerals have different origins, structures, and chemical compositions, but exhibit similar properties and are used mostly for the same purposes. Samples from the two largest deposits of these minerals in Poland were acquired and subjected to structural, chemical, and crystal analysis. Resources of deposits were evaluated based on the current geological data and the information acquired from the owners of the deposits.

## 2. Geological Setting, Resources, and Uses

The two materials under investigation, despite being of entirely different origin, usually serve the same purposes, i.e., as adsorbents, filler materials, insulation, and lining, and are characterized by similar properties. In Table 1, the properties of typical market products of diatomaceous earth and halloysite under investigation are presented. The geological setting of the two deposits and estimated resources are given in the following subsections.

**Table 1.** Properties of adsorbents made of diatomaceous earth from Jawornik deposit and halloysite from the “Dunino” deposit [5,6].

| Property                         | Diatomaceous Earth | Halloysite |
|----------------------------------|--------------------|------------|
| Moisture content of adsorbent, % | 6                  | 8          |
| Oil sorption, wt. %              | 45                 | 80–100     |
| Typical sorbent grain size, mm   | 0.3–3              | 0.5–2.0    |
| Bulk density, kg/m <sup>3</sup>  | 900                | 800        |
| pH                               | 5.7–8.3            | 7          |

### 2.1. Halloysite

Halloysite belongs to the group of phyllosilicates from the kaolinite subgroup. Unlike other minerals in its group, halloysite has a considerably larger specific surface area and greater ion exchange capacity. It is also characterized by good chemical and thermal resistance in low and moderate temperatures [7].

Nowadays, there are only three large-scale active mines of this raw material in the world [8], which are located in the USA, New Zealand, and Poland; the latter features the open pit halloysite mine “Dunino” Sp. z o.o. near Legnica (Lower Silesian Voivodeship). The Dunino deposit, covering an area of 1.99 ha, was documented in 1996 originally as a deposit of halloysite raw material, and now is classified as a kaolinite raw material. Halloysite from this deposit is a product of the weathering of tertiary basalt rocks. It has the form of a horizontal seam, is homogeneous in composition, and was included in the second group of deposit variability in accordance with Baryszew classification (average variability). The thickness of the deposit ranges from 3.5 to 18.8 m (average 12.2 m). The cap

rock includes: soil, quaternary sandy-loam formations, and weathered basalt with sand with thickness ranging from 1.6 to 7.0 m (average 4.0 m). In the bottom layer, clayey sands and weathered basalt occur [9].

The measured resources of this deposit are 470.63 thousand t, whereas proven reserves account for 374.66 thousand t. The production from this deposit in 2018 amounted to 1350 t [4]. The concession for mining the Dunino deposit is granted to the company until 2029. Currently, the only producer of halloysite in Poland is the Intermark Company, which owns the Dunino deposit.

Halloysite may be used for the following purposes:

1. as an adsorbent for the purification of process gases and liquids [10–12];
2. catalyst in chemical processes (e.g., processing of plastics) [13–15];
3. additive in the combustion of biomass, Refused-derived fuel (RDF), and coal in boilers (reduces slagging and fouling of boiler heating surfaces and prevents the agglomeration processes in fluidized beds) [16,17];
4. polymer composites filler (increases mechanical properties and fire resistance) [18–20];
5. as a slow-release fertilizer and plant protection [21,22];
6. animal feed additive [23–25];
7. paint additive (e.g., controlled release of anti-corrosion agents) [26,27];
8. waste water treatment additive [28,29];
9. component of geosynthetic clay liners [30];
10. slow-release drug delivery system [31,32].

The above non-exhaustive list of halloysite uses makes it a valuable resource in modern applications, particularly in medicine and environmental protection.

## 2.2. Diatomaceous Earth

Diatomaceous earth is the naturally occurring fossilized remains of single-celled aquatic algae called diatoms. It belongs to the group of near pure sedimentary silica rock consisting predominantly of opal. The properties that make diatomite industrially valuable include: light weight, low density, high porosity, high surface area, inertness, and high absorption capacity.

The only occurrence of diatomite rock in Poland is located in the Eastern Carpathians, within the Menilite series of Krosno strata, in the Leszczawka area. The raw material from the deposit is characterized by a 72% concentration of SiO<sub>2</sub>, relatively high density (1.42 g/cm<sup>3</sup>), and relatively low porosity (average 28.5%, maximally 50%). Typical diatomite with silica content above 80% is not found in Poland [4].

Measured resources of diatomite in four deposits in the Leszczawka region (two deposits in Leszczawka and Kuźmina and Jawornik deposits) amount to a little over 10 Mt (Tables 2 and 3). The recoverable reserves of diatomite rock for the Leszczawka area are estimated at up to 10 Mt. Much larger prospects for the discovery of diatomite deposits are associated with the Menilite series of Krosno strata in the regions of Błazowa-Piątkowa-Harta-Bachórz and Godów (Rzeszów region) and in the Dydnia-Krzywe region (Krosno region).

**Table 2.** Diatomaceous earth resources of Poland (Mt) [4].

|                                | Amount of Deposits | Measured Resources |                        | Recoverable Reserves |
|--------------------------------|--------------------|--------------------|------------------------|----------------------|
|                                |                    | Total              | Sub-Economic Resources |                      |
| Total resources                | 4                  | 10.02              | 2.74                   | 0.2                  |
| Deposits with active mining    | 1                  | 0.64               | -                      | 0.2                  |
| Deposits with abandoned mining | 3                  | 9.38               | 2.74                   | -                    |

**Table 3.** List of diatomaceous earth deposits in Poland (thousand t) [4].

| No | Deposit                                 | Current status | Measured Resources |                        | Recoverable Reserves | Production |
|----|---|----------------|--------------------|------------------------|----------------------|------------|
|    |   |                | Total              | Sub-Economic Resources |                      |            |
| 1  | Jawornik                                | In operation   | 10,015.93          | 2738                   | 200.10               | 0.58       |
| 2  | Kuźmina                                 | Abandoned      | 640.10             | 2738                   | 200.10               | 0.58       |
| 3  | Leszczawka-pole<br>Jaworowice-Borownica | Abandoned      | 392.19             | -                      | -                    | -          |
| 4  | Leszczawka-pole Kuźmina                 | Abandoned      | 3490               | -                      | -                    | -          |
|    |   |                | 5493.64            | -                      | -                    | -          |

At present, the only domestic producer of diatomite materials is the Specjalistyczne Przedsiębiorstwo Górnicze “Górtech” Sp. z o.o., excavating the Jawornik diatomite deposit since 1992 in the Jawornik Ruski mine. The production of diatomaceous earth from this deposit in 2018 amounted to 0.58 thousand t (see Table 3). The company supplies raw material in the form of 0.5–3 mm granules (used as a sorbent), powder (used as natural mineral filler), and dusts (for the production of insulation materials). Diatomite uses are as follows:

1. carrier of drug, particularly Nonsteroidal Anti-Inflammatory Drugs (NSAID) [33,34];
2. production of antibacterial composites [35–38];
3. filler in cement, asphalt, paint, brick, tile, and ceramics production [39–43];
4. filtration of impurities [44–47];
5. sound and heat insulation composites manufacturing [48–50];
6. thermal storage [51–53].

There are other numerous applications of diatomite, yet the most important property of the deposit should be the purity of resource and lack of organic impurities.

### 3. Materials and Methods

In order to evaluate structure, chemical composition, and properties of halloysite from the Dunino deposit and diatomite from the Jawornik deposit, a detailed study was conducted. Samples from both deposits were subjected to the following set of analyses:

- structural—using light microscopy (LM),
- microstructural and nanostructural—using scanning electron microscopy (SEM),
- elemental—using energy-dispersive X-ray spectroscopy (EDS),
- chemical composition—using the X-ray fluorescence method (XRF) and inductively coupled plasma-optical emission spectrometer (ICP-OES),
- mineral composition—with the use of the X-ray diffraction (XRD) method.

For the purpose of the study, 30 samples of each mineral were used. First, samples were hand crushed and sieved in order to remove large impurities (>30 mm). Before starting the set of analysis, samples were dried in an oven at 105 °C for 2–3 h (until the weight was equilibrated). After drying, samples were placed in a desiccator. SEM-EDS analysis was performed on 20 samples, whereas for LM analysis, 10 samples were used. For the XRD analysis, raw and dry halloysite was used, as well as a dry diatomaceous earth sample.

The selection of research areas for metallographic observations was done after previous macroscopic observations by using a light stereoscopic microscope SteREO Discovery ZEISS in a magnification range from 8× to 100×. A Zeiss stereoscopic microscope was equipped with the two-channel optical observation system, which allowed the observation of spatial objects with a large depth. The microscope was also equipped with directional and annular lighting and the data acquisition and image analysis system called Axio Vision.

The surface morphology of the samples prepared from all the supplied pipes was observed using the high-resolution scanning electron microscope Zeiss Supra 35, which was equipped with an analysis system of the chemical composition with the energy-dispersive X-ray spectroscopy (EDS) TRIDENT XM4 EDAX. The energy-dispersive X-ray spectroscopy (EDS) allowed studying the chemical composition of the samples in the micro areas as well as an analysis of the distribution of elements in large areas. In addition, an analysis of the distribution of elements on the surface of the tested samples and the topographic investigations of the surface were carried out.

Since minerals from halloysite and diatomite deposits are classified as weakly conducting or non-conductive samples to obtain better quality SEM images, their surface was covered with a thin metallic layer of Pd and Au. This prevents disturbances of secondary electron emissions or electron beam emissions. All samples were attached to the scanning microscope handle using a conductive carbon tape. This can explain the occurrence on some EDS single spectrum of individual peaks derived from gold, palladium, and carbon. In the supplied tables, the quantitative and qualitative analyses of these elements were omitted.

Chemical analysis was conducted with the use of a Varian 710-ES inductively coupled plasma-optical emission spectrometer (ICP-OES). Prior to the measurements, samples were mineralized in a Magnum II ERTEC mineralizer. A more detailed chemical composition was established by means of the X-ray fluorescence (XRF) method using the Epsilon 1 spectrometer manufactured by PANalytical.

As mentioned above, X-ray diffraction (XRD) phase analysis was conducted for halloysite and diatomaceous earth samples. This research was conducted with the use of an XRD 7 diffractometer Seifert-FPM. The applied emission was Co K-alpha with an Fe filter. The X-ray tube parameters were 35 kV/25mA with the scattering angle of  $2\theta$  (from  $4^\circ$  for halloysite and  $7^\circ$  for diatomaceous earth) for phase analysis up to  $70\text{--}90^\circ$ .

## 4. Results

### 4.1. Halloysite

Since halloysite is a volcanic-derived mineral formed as a result of basalt weathering, in one of the LM photos, a transformation between basalt and halloysite is visible (Figure 1). Areas of basalt rock (black and grey color) weathered into aluminosilicates (yellowish color) and mainly iron oxides inclusions (reddish color) can be observed.

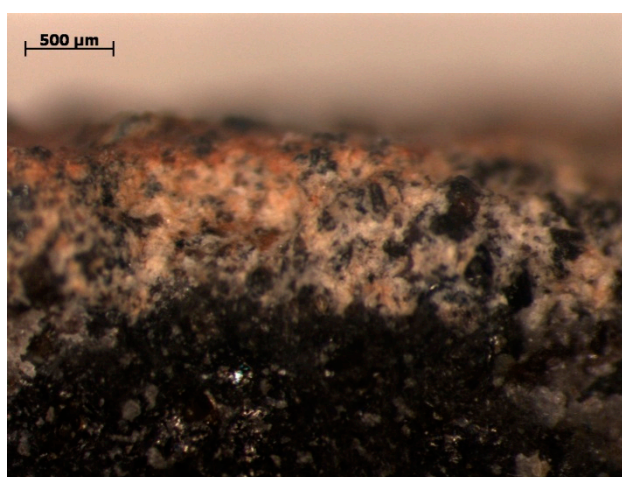


**Figure 1.** Halloysite sample with visible transformation from basalt rock (LM).

All samples exhibited the presence of magnetite particles surrounded by aluminosilicate crystals. Magnetite particles have an average size of  $30\text{--}60\ \mu\text{m}$  up to  $500\ \mu\text{m}$  for the largest particles.

Hematite particles of size not exceeding a few micrometers were also observed. The size of the hematite particles was noticeably smaller than that of the magnetite particles (see Figure 2).

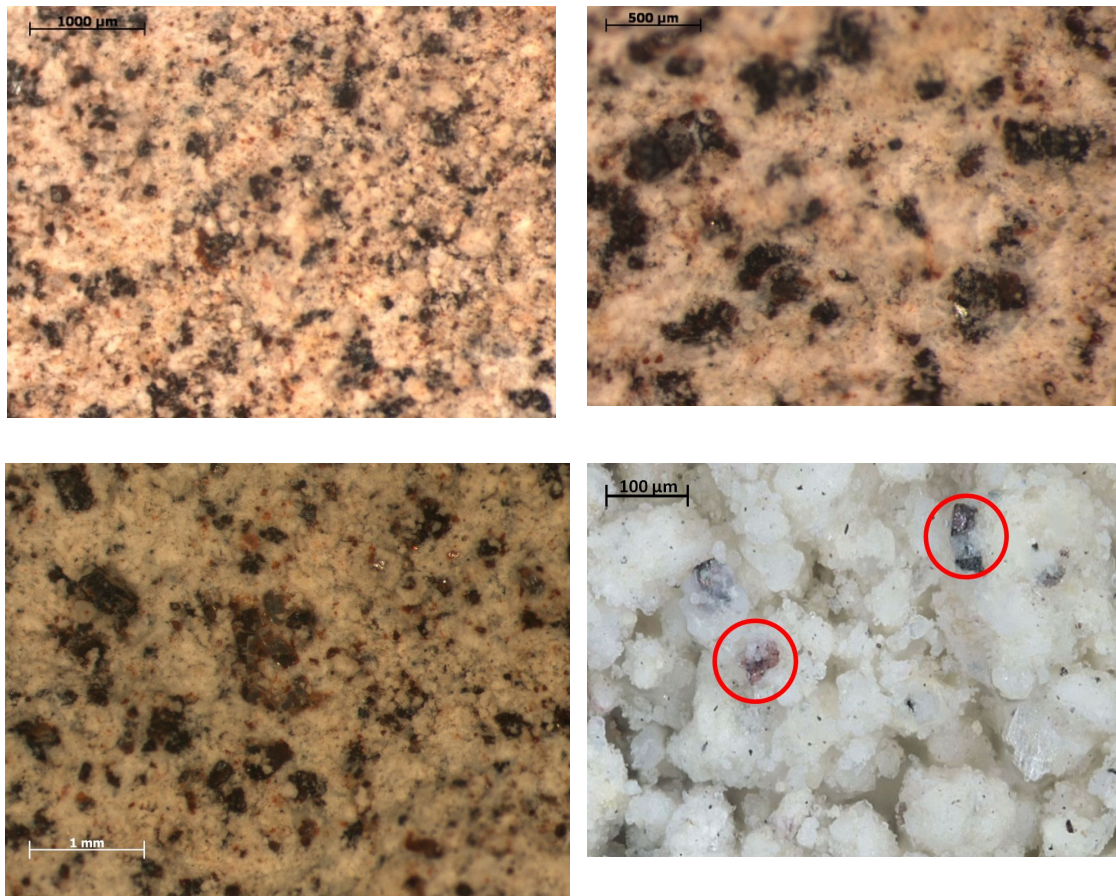


**Figure 2.** The structure of mineral from the Dunino deposit (LM). Selected samples from different areas of deposit with visible hematite and magnetite grains of various sizes (red circles).

Microstructural and nanostructural analysis with the use of SEM showed interesting phenomenon in some of the halloysite samples. In several specimens, halloysite nanoplates (HNP) (Figure 3a) and mixed halloysite nanotubes (HNT) and halloysite nanoplates (HNP) occur (Figure 3b,c).

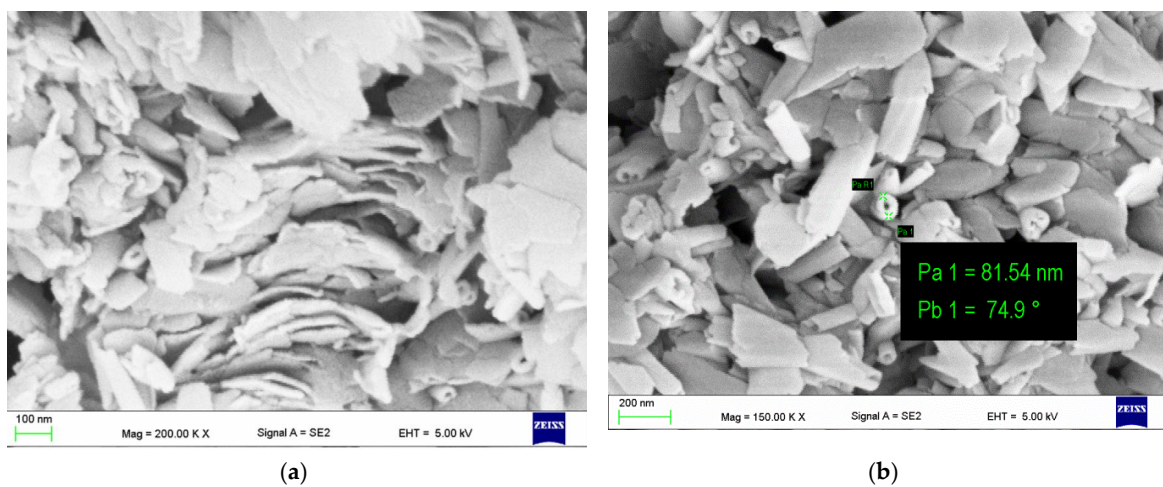
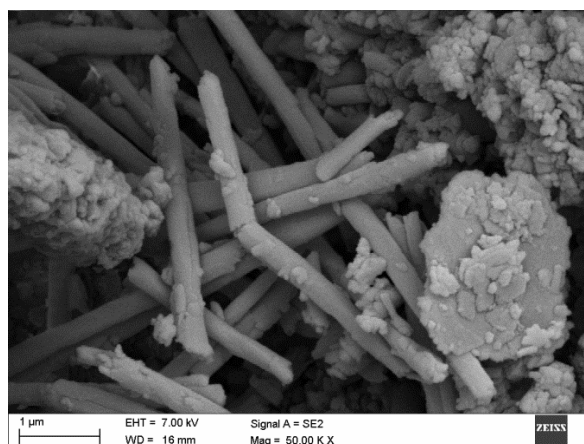


**Figure 3.** Cont.



(c)

**Figure 3.** SEM images Dunino halloysite samples with (a) halloysiteite nanoplates (HNP) with an occasional intrusion of nanotubes (HNT); (b,c) mixed halloysiteite nanotubes (HNT) and halloysiteite nanoplates.

EDS elemental analysis were conducted for 30 samples of halloysite from the Dunino deposit. The mass-averaged quantitative and qualitative EDS elemental analysis showed that the most important elements found are: oxygen, aluminum, silica, iron, and titanium. The arithmetic mean of the analyses is given in the Table 4. The differences resulting from the theoretical content of individual elements may result from the heterogeneity of composition and the occurrence of inclusions in the form of particles and grains as well as numerous substitutions of iron and titanium atoms in the halloysite crystals themselves.

**Table 4.** Averaged mass percentage concentrations of the major elements in dried Dunino halloysite (energy-dispersive X-ray spectroscopy (EDS) analysis).

| Element | Mass (%) |
|---------|----------|
| O       | 43.4     |
| Si      | 19.4     |
| Al      | 18.6     |
| Fe      | 12.8     |
| Ti      | 1.41     |

Elemental analysis showed that the Dunino deposit is macroscopically homogeneous; however, in micro-areas, there are local fluctuations in chemical composition due to the volcanic origin of the mineral. Local differences in the chemical composition may be the result of individual eruptions, and as a consequence, different compositions of basalt rock. In Figures 4 and 5, SEM micrograph and EDS results show differences in the chemical composition of the samples. In Figure 5, an iron oxide impurity is found with a high content of FeK, whereas in Figure 4, the same sample shows a chemical composition that is typical for halloysite. The chemical composition of halloysite measured with ICP-OES is shown in Table 5, and is consistent with results obtained with EDS.

**Table 5.** Averaged chemical composition of halloyiste from Dunino deposit using an inductively coupled plasma-optical emission spectrometer (ICP-OES).

| Compound | SiO <sub>2</sub> | Al <sub>2</sub> O <sub>3</sub> | Fe <sub>2</sub> O <sub>3</sub> | TiO <sub>2</sub> | Na <sub>2</sub> O | K <sub>2</sub> O | CaO | MgO | Loss on Ignition |
|----------|------------------|--------------------------------|--------------------------------|------------------|-------------------|------------------|-----|-----|------------------|
| (wt.%)   | 33               | 28                             | 18                             | 2                | 0.1               | 0.1              | 1.3 | 0.5 | 15               |

Additional XRF analysis (Table 6) show that the chemical composition is consistent with the results obtained with ICP-OES. The dominant trace elements found in halloysite are zirconium, vanadium, and chromium, yet maximum concentrations do not exceed 150 ppm.

**Table 6.** Chemical composition and trace elements of halloysite determined by means of the X-ray fluorescence method.

| Compound                       | wt. % | Element | Concentration, ppm |
|--------------------------------|-------|---------|--------------------|
| SiO <sub>2</sub>               | 33.11 | V       | 124.9              |
| TiO <sub>2</sub>               | 2.23  | Cr      | 103                |
| Al <sub>2</sub> O <sub>3</sub> | 28.87 | Ni      | 36.1               |
| Fe <sub>2</sub> O <sub>3</sub> | 17.92 | Cu      | 73.8               |
| MnO                            | 0.48  | Zn      | 84                 |
| MgO                            | 0.14  | Ga      | 16.9               |
| CaO                            | 0.71  | As      | 8.2                |
| Na <sub>2</sub> O              | 0     | Rb      | 131                |
| K <sub>2</sub> O               | 0.14  | Sr      | 96.3               |
| P <sub>2</sub> O <sub>5</sub>  | 0.77  | Y       | 28.8               |
| SO <sub>3</sub>                | 0     | Zr      | 180.9              |
| Cl                             | 0.05  | Nb      | 10.9               |
| BaO                            | 0.08  | Mo      | 4.1                |
| LOI                            | 15    | Sn      | 37.1               |
|                                |       | Pb      | 7                  |

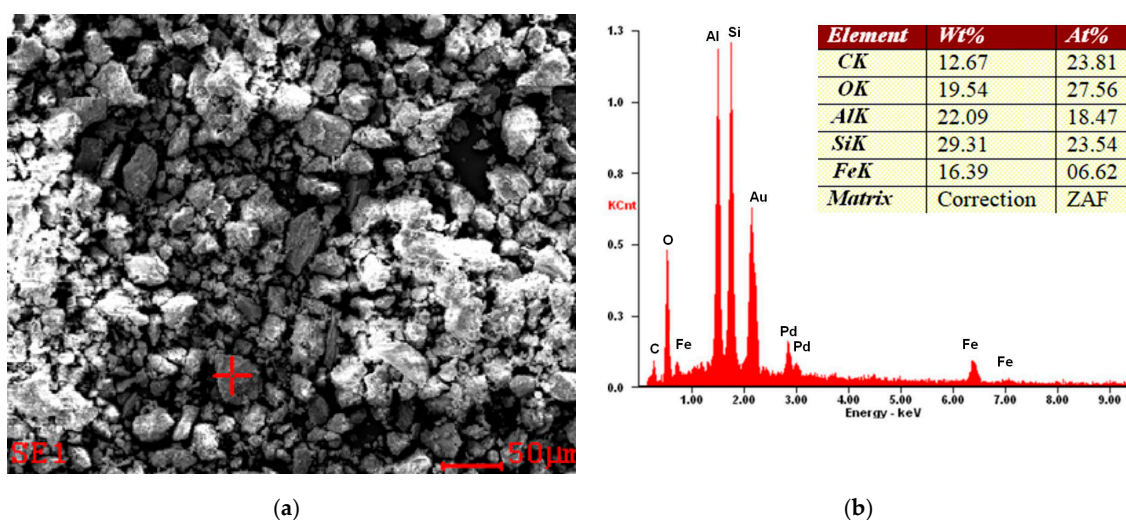


**Figure 4.** Example of SEM micrograph (a) and EDS spectra (b) of a halloysite sample from the Dunino deposit. The sample was sputtered by an Au/Pd target.

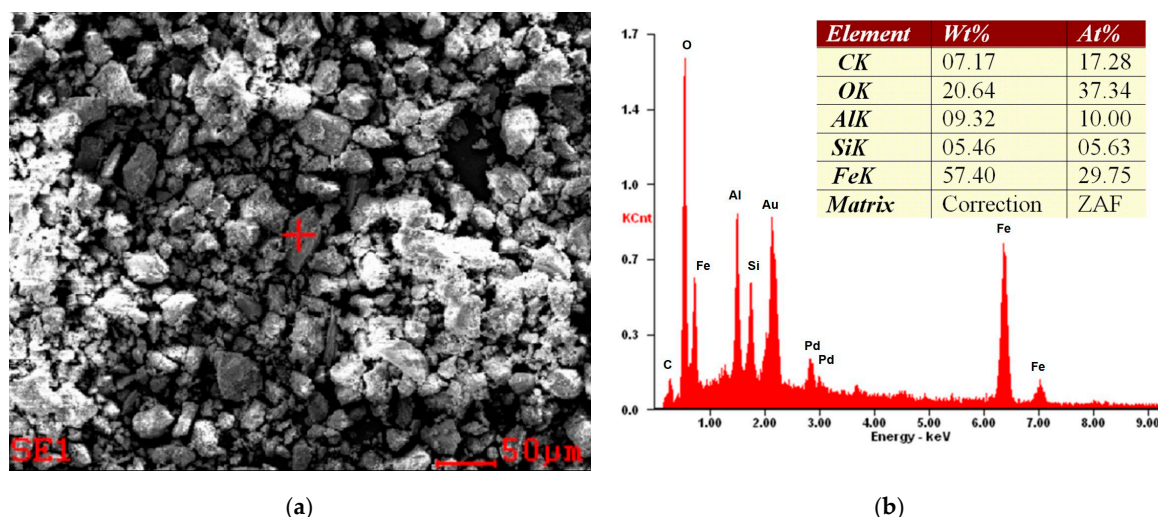


**Figure 5.** Example of SEM micrograph (a) and EDS spectra (b) of the halloysite sample from the Dunino deposit. The sample was sputtered by the Au/Pd target. EDS results indicate impurity, probably in the form of the iron compound.

With the use of X-Ray diffraction, the following minerals were identified (Figure 6): halloysite, kaolinite, hematite, magnetite, quartz, magnesioferrite, rutile, ilmenite, geikielite, goyazite, gorceixite, and crandallite.

The halloysite sample from the Dunino deposit is a type of aluminasilicate clay where the basic structural unit is a single crystal surrounded by a silica tetrahedral sheet and the other alumina octahedral sheet. Between these layers, the interlayer water exists (Figure 7). A raw sample of halloysite was dehydrated during drying, and the 10Å halloysite has been irreversibly changed into the 7Å halloysite. In the diffractograms of Dunino halloysite samples, the peaks of both the raw  $[Al_2(OH)_4Si_2O_5 \cdot 2H_2O]$  and dried  $[Al_2(OH)_4Si_2O_5]$  halloysite are shown (see Figure 6).

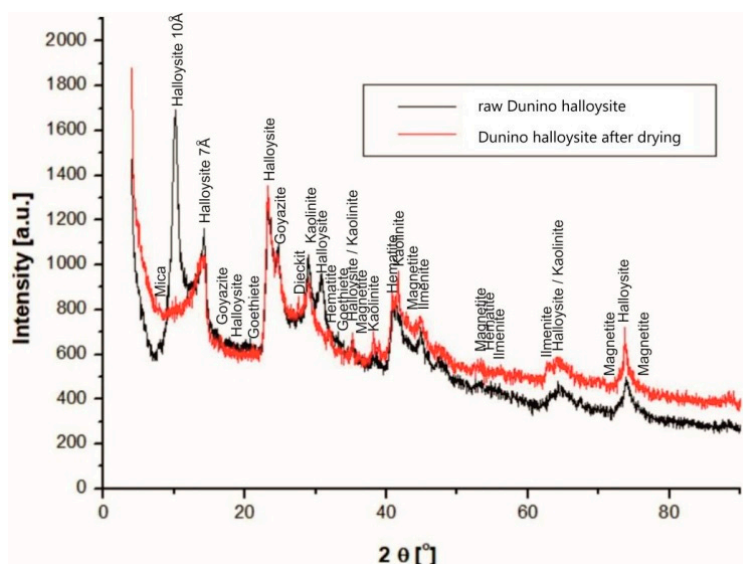


**Figure 6.** X-ray diffraction (XRD) patterns of raw halloysite and dried halloysite from the Dunino deposit.

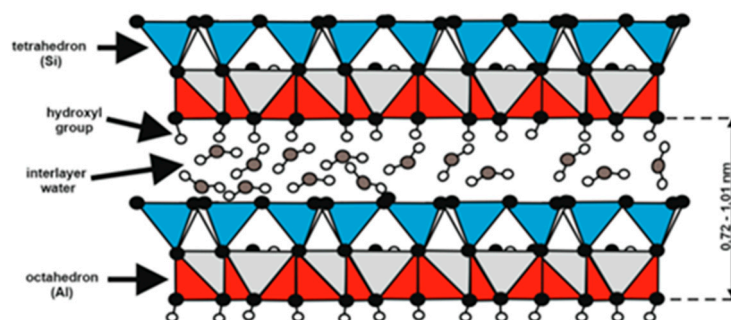


**Figure 7.** Single crystal structure of halloysite from the Dunino deposit.

#### 4.2. Diatomaceous Earth

A mineralogical investigation of a diatomaceous earth sample from Jawornik, using light microscopy and SEM analysis, showed that the sample is composed of diatomaceous skeletons (frustules), clay minerals (kaolinite, illite, and smectites), quartz, iron oxides (impurities), a small amount of feldspars, and organic matter (Figures 8 and 9).

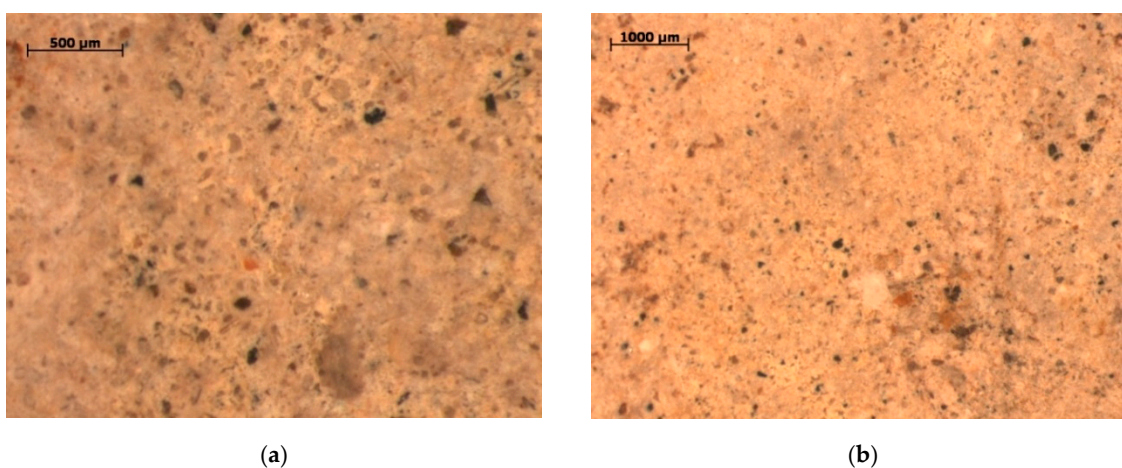


**Figure 8.** The structure of diatomaceous earth from the Jawornik deposit (LM). Dark areas show iron oxide impurities (a), whereas orange areas show clay minerals, and white are quartz particles (b).

SEM images showed that the frustules are mostly centric (discoid) without an abundant occurrence of pinnate forms. Diatoms have a radius of approximately 50–60 μm. As it can be seen from Figure 9b, diatoms have a highly porous structure. The pores size on the frustule walls ranged from 100 to 200 nm. Previous studies showed that amorphous silica fills some pores of a diatom frustule, whereas others are partially dissolved [54]; in our observations, we did not encounter that phenomenon. On some of the SEM images, detrital grains are visible (Figure 9a). The majority of identified frustule species were discoid frustules from the family *Thalassiosiraceae* and cylindrical *Aulacoseira islandica* (upper right corner of Figure 9a).

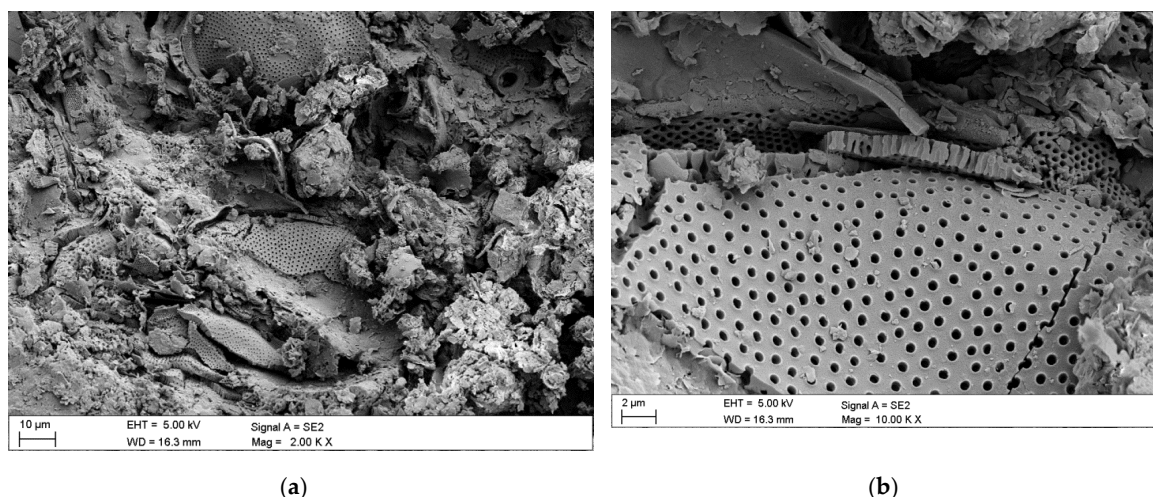


**Figure 9.** SEM images of microstructure and nanostructure of diatomaceous earth from the Jawornik deposit. (a) View of a raw diatomaceous earth sample, (b) close-up of the porous structure of a single frustule.

The elemental analysis made by the energy-dispersive X-ray spectroscopy (EDS) in micro-areas on the surface of diatomaceous earth from the Jawornik deposit show differences in the qualitative and quantitative chemical composition of the minerals. The mass-averaged quantitative and qualitative EDS elemental analysis showed that the most important elements found are: oxygen, silicon, aluminum, and iron. The averaged mass percentage concentrations of the major elements in diatomaceous earth are shown in Table 7.

**Table 7.** Averaged mass percentage concentrations of the major elements in diatomaceous earth (EDS analysis).

| Element | Mass (%) |
|---------|----------|
| O       | 48.4     |
| Si      | 45.7     |
| Al      | 3.2      |
| Fe      | 2.7      |

The elemental composition of diatomaceous earth based on the EDS analysis is consistent with chemical composition (Table 8).

**Table 8.** Chemical composition of diatomaceous earth from the Jawornik deposit.

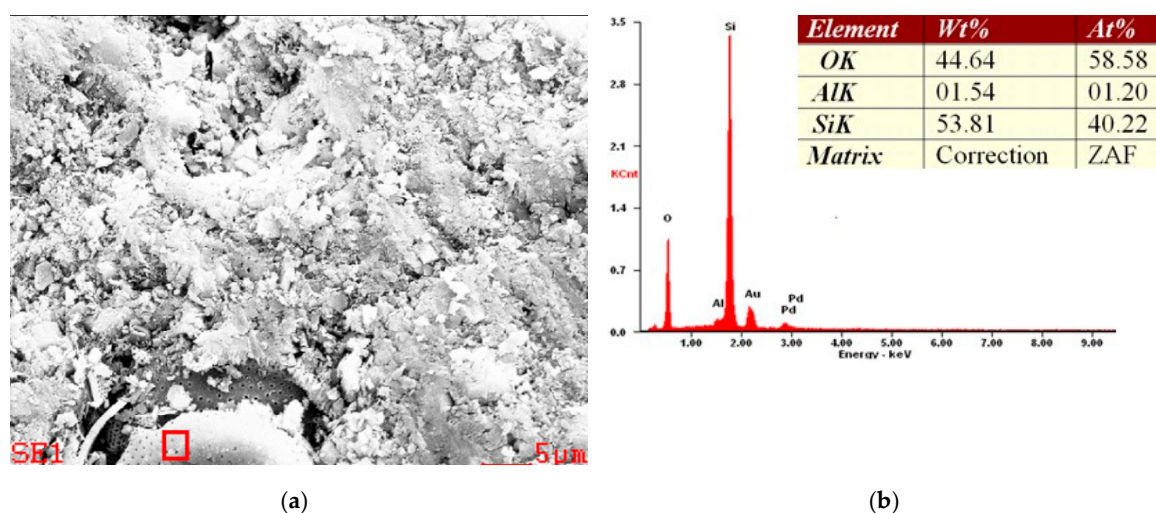
| Compound | SiO <sub>2</sub> | Al <sub>2</sub> O <sub>3</sub> | Fe <sub>2</sub> O <sub>3</sub> | TiO <sub>2</sub> | Na <sub>2</sub> O | K <sub>2</sub> O | CaO | MgO  | Loss on Ignition |
|----------|------------------|--------------------------------|--------------------------------|------------------|-------------------|------------------|-----|------|------------------|
| (wt.%)   | 69.2             | 11.8                           | 4.3                            | 0.5              | 0.15              | 1.24             | 1.2 | 0.75 | 10.86            |

In order to confirm the ICP-OES chemical composition results, additional XRF analyses were also performed for the diatomaceous earth samples (Table 9). The chemical composition was consistent with results obtained with ICP-OES and matched the identified minerals in XRD. The dominant trace elements found in halloysite were chromium, nickel, and vanadium with concentration reaching almost 800 ppm. The concentration of these elements is considerably higher than in halloysite.

**Table 9.** Chemical composition and trace elements of diatomaceous earth determined by means of the X-ray fluorescence method.

| Compound                       | wt. % | Element | Concentration, ppm |
|--------------------------------|-------|---------|--------------------|
| SiO <sub>2</sub>               | 68.16 | V       | 349.8              |
| TiO <sub>2</sub>               | 0.51  | Cr      | 776.8              |
| Al <sub>2</sub> O <sub>3</sub> | 10.95 | Bi      | 8.8                |
| Fe <sub>2</sub> O <sub>3</sub> | 4.57  | Ni      | 746.8              |
| MnO                            | 0.04  | Cu      | 0                  |
| MgO                            | 0.82  | Zn      | 211.7              |
| CaO                            | 0.46  | Ga      | 37.3               |
| Na <sub>2</sub> O              | 0.3   | Rb      | 35.4               |
| K <sub>2</sub> O               | 2.23  | Sr      | 191.5              |
| P <sub>2</sub> O <sub>5</sub>  | 0.4   | Y       | 131.4              |
| SO <sub>3</sub>                | 0.49  | Zr      | 404.7              |
| Cl                             | 0.07  | Nb      | 77.5               |
| BaO                            | 0.02  | Mo      | 7.4                |
| LOI                            | 10.86 | Sn      | 67                 |
|                                |       | Ta      | 0                  |

An example of the EDS results are shown in Figures 10–12. Figures 10 and 11 show the typical elemental composition of diatom, whereas Figure 12 shows iron oxide impurity.

**Figure 10.** Example of SEM micrograph (a) and EDS spectra (b) of a diatomaceous earth sample from the Jawornik deposit. The sample was sputtered by an Au/Pd target.

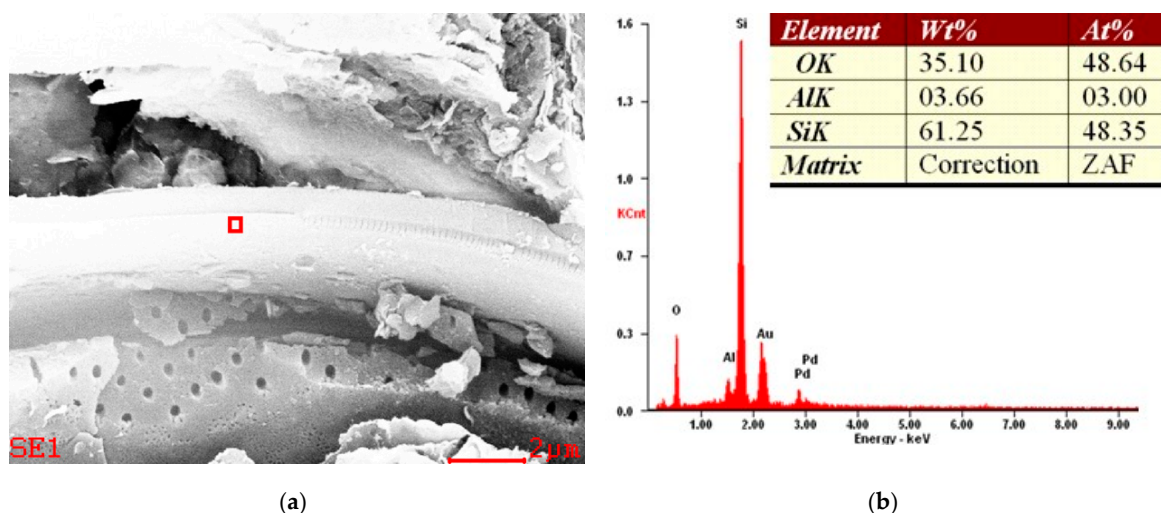


**Figure 11.** Example of SEM micrograph (a) and EDS spectra (b) of a diatomaceous earth sample from the Jawornik deposit. The sample was sputtered by an Au/Pd target.

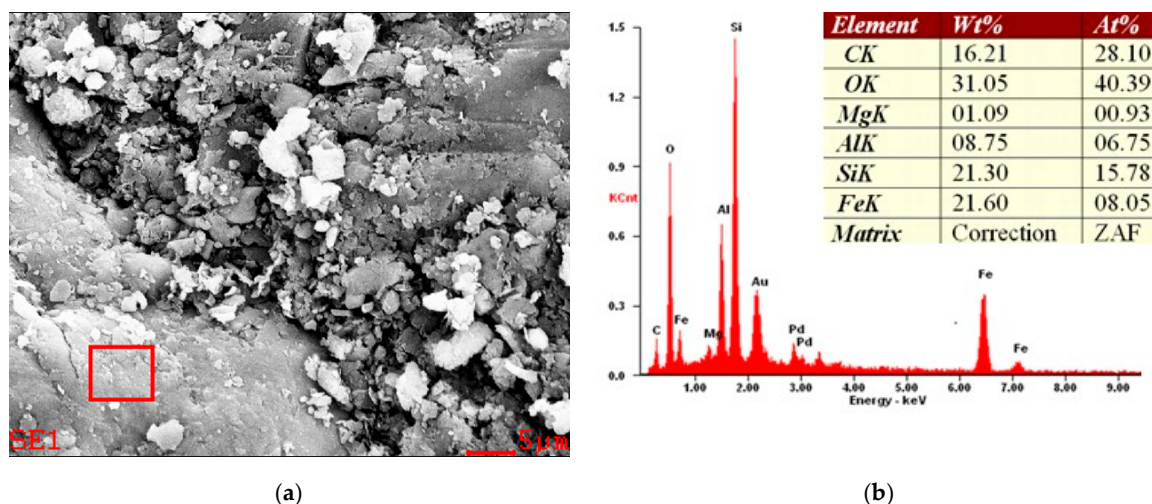


**Figure 12.** Example of SEM micrograph (a) and EDS spectra (b) of a diatomaceous earth sample from the Jawornik deposit.

The XRD of the diatomaceous earth sample (Figure 13) depicted crystalline peaks of silica-containing phases (quartz, opal) and clay minerals (illite and kaolinite).

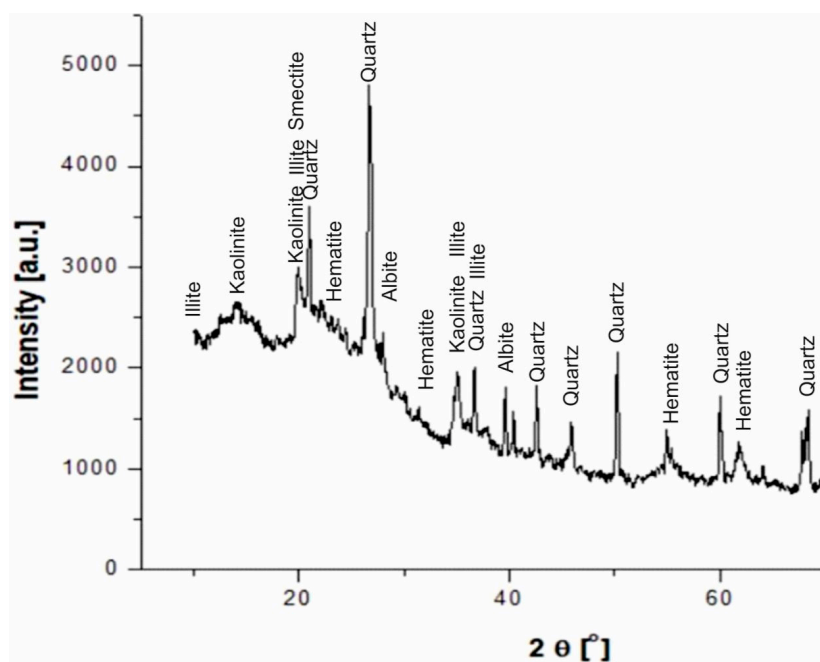


Figure 13. X-ray diffraction patterns of a raw diatomite sample from the Jawornik deposit.

## 5. Discussion

The results of the analysis show that both deposits are rather homogeneous; however, impurities in the form of iron oxides or organic matter can be found. This is evident since materials for the tests were not subjected to any upgrading method or impurities removal. The most common method of halloysite and diatomaceous earth processing is calcination at 650 °C and 900–1000 °C, respectively. This process develops the specific surface of these minerals and enhances their sorption capacity [55–58]. Other methods that could be applied include surface modification or purification, particularly in the case of halloysite [59,60]. Both of these minerals have similar properties and could be used interchangeably.

These two raw materials from deposits located in Poland are abundant and easily accessible. The mining of these minerals is cost-efficient (open-pit mining at shallow depths with the use of an excavator), and does not disturb the environment, as in the case of deep open-pit mining. Large resources of these minerals could be used in the future either for manufacturing composite materials or for environmental purposes. This is particularly important given the fact that the mining industry is declining in the European Union, and the share of raw materials imported to the EU is increasing. The above-mentioned examples show that such deposits could be the future of the extractive industry in Europe.

**Author Contributions:** As a corresponding author, M.L. conceptualized the work, elaborated the methodology, and wrote the major part of the article along with reviewing and editing. P.S. did the investigation, performed the experiments and analysis, along with the interpretation of results. S.L. did the description of geological setting and resources, gathered and interpreted data, and contributed to writing and editing the article.

**Acknowledgments:** We would like to thank “Dunino” Sp. z o.o. and “Górtech” Sp. z o.o. for manufacturing the DIATO sorbent for access and providing the data for the article.

**Conflicts of Interest:** The authors declare no conflict of interest.

## References

1. Cassard, D.; Leistel, J.; Lips, A.L.W.; Stein, G. *Metallogenic Map of Central and Southeastern Europe: An Extract from GIS Central Europe*; Intermediary Report; BRGM/RP-54703-FR; BRGM: Paris, France, 2008.
2. Martínón-Torres, M.; Rehren, T. *Archaeology, History and Science: Integrating Approaches to Ancient Materials*; Left Coast Press: Walnut Creek, CA, USA, 2009; ISBN 978-1-59874-350-0.

3. Pollard, S. *Marginal Europe: The Contribution of Marginal Lands since the Middle Ages*; Clarendon Press: Oxford, UK; New York, NY, USA, 1997; ISBN 978-0-19-820638-5.
4. Szufflicki, M.; Malon, A.; Tymiński, M. *Bilans Zasobów Złóż Kopalin w Polsce wg Stanu na 31 XII 2018 r*; Państwowy Instytut Geologiczny—Państwowy Instytut Badawczy: Warszawa, Poland, 2019.
5. Material Safety Data Sheet. "HALOSORB" *Universal Mineral Adsorbent*; PTH Intermark: Gliwice, Poland, 2016.
6. Material Safety Data Sheet. *Diatomite Sorbent*; Specjalistyczne Przedsiębiorstwo Górnicze "Górzech" Sp. z o. o.: Kraków, Poland, 2018.
7. Matusik, J. *Minerały z Grupy Kaolinitu Jako Prekursory Nanorurek Mineralnych*. Ph.D. Thesis, AGH University of Science and Technology, Krakow, Poland, 2010.
8. Keeling, J.L. *The Mineralogy, Geology and Occurrences of Halloysite*; Apple Academic Press: Oakville, ON, Canada, 2015.
9. Bogacz, A.; Kawulak, M.; Poręba, E.; Lis, J. *Objaśnienia do Mapy Geośrodowiskowej Polski Arkusz Jawor 760*; Państwowy Instytut Geologiczny—Państwowy Instytut Badawczy: Warszawa, Poland, 2004.
10. Hardy, T.; Kordylewski, W.; Mościcki, K. Use of aluminosilicate sorbents to control KCl vapors in biomass combustion gases. *J. Power Technol.* **2013**, *93*, 37–43.
11. Cheng, A.-L.; Huang, W.-L. Selective adsorption of hydrocarbon gases on clays and organic matter. *Org. Geochem.* **2004**, *35*, 413–423. [[CrossRef](#)]
12. Volzone, C.; Thompson, J.G.; Melnitchenko, A.; Ortiga, J.; Palethorpe, S.R. Selective gas adsorption by amorphous clay-mineral derivatives. *Clays Clay Miner.* **1999**, *47*, 647–657. [[CrossRef](#)]
13. Cho, K.-H.; Jang, B.-S.; Kim, K.-H.; Park, D.-W. Performance of pyrophyllite and halloysite clays in the catalytic degradation of polystyrene. *React. Kinet. Catal. Lett.* **2006**, *88*, 43–50. [[CrossRef](#)]
14. Shah, J.; Jan, M.R. Polystyrene degradation studies using Cu supported catalysts. *J. Anal. Appl. Pyrolysis* **2014**, *109*, 196–204.
15. Tae, J.-W.; Jang, B.-S.; Kim, J.-R.; Kim, I.; Park, D.-W. Catalytic degradation of polystyrene using acid-treated halloysite clays. *Solid State Ion.* **2004**, *172*, 129–133. [[CrossRef](#)]
16. Selvakumaran, P.; Lawrence, A.; Bakthavatsalam, A.K. Effect of additives on sintering of lignites during CFB combustion. *Appl. Therm. Eng.* **2014**, *67*, 480–488. [[CrossRef](#)]
17. Mroczek, K.; Kalisz, S.; Pronobis, M.; Sołtys, J. The effect of halloysite additive on operation of boilers firing agricultural biomass. *Fuel Process. Technol.* **2011**, *92*, 845–855. [[CrossRef](#)]
18. Abdullayev, E.; Lvov, Y. Halloysite clay nanotubes as a ceramic "skeleton" for functional biopolymer composites with sustained drug release. *J. Mater. Chem. B* **2013**, *1*, 2894–2903. [[CrossRef](#)]
19. De Silva, R.T.; Pasbakhsh, P.; Goh, K.L.; Chai, S.-P.; Ismail, H. Physico-chemical characterisation of chitosan/halloysite composite membranes. *Polym. Test.* **2013**, *32*, 265–271. [[CrossRef](#)]
20. Cui, Y.; Kumar, S.; Kona, B.R.; van Houcke, D. Gas barrier properties of polymer/clay nanocomposites. *RSC Adv.* **2015**, *5*, 63669–63690. [[CrossRef](#)]
21. Subramanian, K.S.; Sharmila Rahale, C. Ball milled nanosized zeolite loaded with zinc sulfate: A putative slow release Zn fertilizer. *Int. J. Innov. Hortic.* **2012**, *1*, 33–40.
22. Borges, R.; Brunatto, S.F.; Leitão, A.A.; De Carvalho, G.S.; Wypych, F. Solid-state mechanochemical activation of clay minerals and soluble phosphate mixtures to obtain slow-release fertilizers. *Clay Miner.* **2015**, *50*, 153–162. [[CrossRef](#)]
23. Kulok, M.; Kołacz, R.; Dobrzański, Z.; Wolska, I. The influence of halloysite on the content of bacteria, fungi and mycotoxins in feed mixtures. In Proceedings of the XIIth International Society for Animal Hygiene Congress, Warsaw, Poland, 4–8 September 2005; Volume 2, pp. 354–357.
24. Korniewicz, D.; Kołacz, R.; Dobrzański, Z.; Korniewicz, A.; Kulok, M. Effect of dietary halloysite on the quality of feed and utilization of nutrients by fatteners. *EJPAU Anim. Husb.* **2006**, *9*, 59.
25. Skiba, M.; Kulok, M.; Kołacz, R.; Skiba, T. The influence of halloysite supplementation in laying hens feeding on egg yolk lipid fraction. In *World Poultry Science Association, Proceedings of the 19th European Symposium on Quality of Poultry Meat, 13th European Symposium on the Quality of Eggs and Egg Products, Turku, Finland, 21–25 June 2009*; World's Poultry Science Association (WPSA): Beekbergen, The Netherlands, 2009; pp. 1–9.
26. Abdullayev, E.; Price, R.; Shchukin, D.; Lvov, Y. Halloysite tubes as nanocontainers for anticorrosion coating with benzotriazole. *ACS Appl. Mater. Interfaces* **2009**, *1*, 1437–1443. [[CrossRef](#)] [[PubMed](#)]

27. Abdullayev, E.; Abbasov, V.; Tursunbayeva, A.; Portnov, V.; Ibrahimov, H.; Mukhtarova, G.; Lvov, Y. Self-healing coatings based on halloysite clay polymer composites for protection of copper alloys. *ACS Appl. Mater. Interfaces* **2013**, *5*, 4464–4471. [[CrossRef](#)] [[PubMed](#)]
28. Shabeer, T.A.; Saha, A.; Gajbhiye, V.T.; Gupta, S.; Manjaiah, K.M.; Varghese, E. Exploitation of nano-bentonite, nano-halloysite and organically modified nano-montmorillonite as an adsorbent and coagulation aid for the removal of multi-pesticides from water: A sorption modelling approach. *Water Air Soil Pollut.* **2015**, *226*, 41. [[CrossRef](#)]
29. Shabeer, T.A.; Saha, A.; Gajbhiye, V.T.; Gupta, S.; Manjaiah, K.M.; Varghese, E. Removal of poly aromatic hydrocarbons (PAHs) from water: Effect of nano and modified nano-clays as a flocculation aid and adsorbent in coagulation-flocculation process. *Polycycl. Aromat. Compd.* **2014**, *34*, 452–467. [[CrossRef](#)]
30. Sakiewicz, P.; Nowosielski, R.; Pilarczyk, W.; Gołombek, K.; Lutyński, M. Selected properties of the halloysite as a component of Geosynthetic Clay Liners (GCL). *J. Achiev. Mater. Manuf. Eng.* **2011**, *48*, 177–191.
31. Levis, S.R.; Deasy, P.B. Characterisation of halloysite for use as a microtubular drug delivery system. *Int. J. Pharm.* **2002**, *243*, 125–134. [[CrossRef](#)]
32. Veerabadran, N.G.; Price, R.R.; Lvov, Y.M. Clay nanotubes for encapsulation and sustained release of drugs. *Nano* **2007**, *2*, 115–120. [[CrossRef](#)]
33. Aw, M.S.; Simovic, S.; Addai-Mensah, J.; Losic, D. Silica microcapsules from diatoms as new carrier for delivery of therapeutics. *Nanomedicine* **2011**, *6*, 1159–1173. [[CrossRef](#)] [[PubMed](#)]
34. Janićijević, J.; Milić, J.; Čalića, B.; Micov, A.; Stepanović-Petrović, R.; Tomić, M.; Daković, A.; Dobričić, V.; Vasiljević, B.N.; Krajišnik, D. Potentiation of the ibuprofen antihyperalgesic effect using inorganically functionalized diatomite. *J. Mater. Chem. B* **2018**, *6*, 5812–5822. [[CrossRef](#)]
35. Gao, L.; Wang, L.; Yang, L.; Zhao, Y.; Shi, N.; An, C.; Sun, Y.; Xie, J.; Wang, H.; Song, Y.; et al. Preparation, characterization and antibacterial activity of silver nanoparticle/graphene oxide/diatomite composite. *Appl. Surf. Sci.* **2019**, *484*, 628–636. [[CrossRef](#)]
36. Ruíz-Baltazar, Á.J. Green Composite Based on Silver Nanoparticles Supported on Diatomaceous Earth: Kinetic Adsorption Models and Antibacterial Effect. *J. Clust. Sci.* **2018**, *29*, 509–519. [[CrossRef](#)]
37. Sun, H.; Wen, X.; Zhang, X.; Wei, D.; Yang, H.; Li, C.; Yang, L. Biocompatible silver nanoparticle-modified natural diatomite with anti-infective property. *J. Nanomater.* **2018**, *2018*. [[CrossRef](#)]
38. Xia, Y.; Jiang, X.; Zhang, J.; Lin, M.; Tang, X.; Zhang, J.; Liu, H. Synthesis and characterization of antimicrobial nanosilver/diatomite nanocomposites and its water treatment application. *Appl. Surf. Sci.* **2017**, *396*, 1760–1764. [[CrossRef](#)]
39. Degirmenci, N.; Yilmaz, A. Use of diatomite as partial replacement for Portland cement in cement mortars. *Constr. Build. Mater.* **2009**, *23*, 284–288. [[CrossRef](#)]
40. Ergün, A. Effects of the usage of diatomite and waste marble powder as partial replacement of cement on the mechanical properties of concrete. *Constr. Build. Mater.* **2011**, *25*, 806–812. [[CrossRef](#)]
41. Ivanov, S.E.; Belyakov, A.V. Diatomite and its applications. *Glass Ceram.* **2008**, *65*, 48–51. [[CrossRef](#)]
42. Li, X.; Bian, C.; Chen, W.; He, J.; Wang, Z.; Xu, N.; Xue, G. Polyaniline on surface modification of diatomite: A novel way to obtain conducting diatomite fillers. *Appl. Surf. Sci.* **2003**, *207*, 378–383. [[CrossRef](#)]
43. Kietzman, J.H.; Rodier, C.E. Effect of diatomite filler on performance of asphalt pavements. *Transp. Res. Rec.* **1984**, *968*, 8–19.
44. Gómez, J.; Gil, M.L.A.; De La Rosa-Fox, N.; Alguacil, M. Formation of siliceous sediments in brandy after diatomite filtration. *Food Chem.* **2015**, *170*, 84–89. [[CrossRef](#)] [[PubMed](#)]
45. Guo, D.; Wang, H.; Fu, P.; Huang, Y.; Liu, Y.; Lv, W.; Wang, F. Diatomite precoat filtration for wastewater treatment: Filtration performance and pollution mechanisms. *Chem. Eng. Res. Des.* **2018**, *137*, 403–411. [[CrossRef](#)]
46. Zhang, X.; Zhang, B.; Wu, Y.; Wang, T.; Qiu, J. Preparation and characterization of a diatomite hybrid microfiltration carbon membrane for oily wastewater treatment. *J. Taiwan Inst. Chem. Eng.* **2018**, *89*, 39–48. [[CrossRef](#)]
47. Puzkarewicz, A.; Kaleta, J. Adsorption of chromium (VI) on raw and modified carpathian diatomite. *J. Ecol. Eng.* **2019**, *20*, 11–17.
48. Gong, J. Investigation of Sound Absorption Properties of Diatomite/Polypropylene Composite Materials. *Jianzhu Cailiao Xuebao*. *Build. Mater.* **2018**, *21*, 678–682.

49. Lin, J.; Guo, J.; Zhao, Y.; Duan, L.; Jin, S. Microstructure and sound absorption property of diatomite/polyurethane porous composites. *Fuhe Cailiao Xuebao/Acta Mater. Compos. Sin.* **2014**, *31*, 1476–1480.
50. Jeong, S.-G.; Jeon, J.; Lee, J.-H.; Kim, S. Optimal preparation of PCM/diatomite composites for enhancing thermal properties. *Int. J. Heat Mass Transf.* **2013**, *62*, 711–717. [[CrossRef](#)]
51. Sun, Z.; Zhang, Y.; Zheng, S.; Park, Y.; Frost, R.L. Preparation and thermal energy storage properties of paraffin/calcined diatomite composites as form-stable phase change materials. *Thermochim. Acta* **2013**, *558*, 16–21. [[CrossRef](#)]
52. Xu, B.; Li, Z. Paraffin/diatomite composite phase change material incorporated cement-based composite for thermal energy storage. *Appl. Energy* **2013**, *105*, 229–237. [[CrossRef](#)]
53. Qian, T.; Li, J.; Min, X.; Guan, W.; Deng, Y.; Ning, L. Enhanced thermal conductivity of PEG/diatomite shape-stabilized phase change materials with Ag nanoparticles for thermal energy storage. *J. Mater. Chem. A* **2015**, *3*, 8526–8536. [[CrossRef](#)]
54. Figarska-Warchoń, B.; Stańczak, G.; Rembiś, M.; Tobała, T. Diatomaceous rocks of the Jawornik deposit (the Polish Outer Carpathians): Petrophysical and petrographical evaluation. *Geol. Geophys. Environ.* **2015**, *41*, 311–331. [[CrossRef](#)]
55. Deng, L.; Yuan, P.; Liu, D.; Du, P.; Zhou, J.; Wei, Y.; Song, Y.; Liu, Y. Effects of calcination and acid treatment on improving benzene adsorption performance of halloysite. *Appl. Clay Sci.* **2019**, *181*, 105240. [[CrossRef](#)]
56. Yuan, P.; Tan, D.; Annabi-Bergaya, F.; Yan, W.; Fan, M.; Liu, D.; He, H. Changes in structure, morphology, porosity, and surface activity of mesoporous halloysite nanotubes under heating. *Clays Clay Miner.* **2012**, *60*, 561–573. [[CrossRef](#)]
57. Ediz, N.; Bentli, İ.; Tatar, İ. Improvement in filtration characteristics of diatomite by calcination. *Int. J. Miner. Process.* **2010**, *94*, 129–134. [[CrossRef](#)]
58. Yusan, S.; Gok, C.; Erenturk, S.; Aytas, S. Adsorptive removal of thorium (IV) using calcined and flux calcined diatomite from Turkey: Evaluation of equilibrium, kinetic and thermodynamic data. *Appl. Clay Sci.* **2012**, *67*, 106–116. [[CrossRef](#)]
59. Sakiewicz, P.; Lutynski, M.; Soltys, J.; Pytlinski, A. Purification of halloysite by magnetic separation. *Physicochem. Probl. Miner. Process.* **2016**, *52*. [[CrossRef](#)]
60. Sakiewicz, P.; Lutynski, M.A. Purification of Dunino halloysite by H<sub>2</sub>SO<sub>4</sub> leaching and magnetic separation. In Proceedings of the E3S Web of Conferences, MEC 2016, Swieradow-Zdroj, Poland, 25–28 September 2016; Volume 8, p. 01032.



© 2019 by the authors. Licensee MDPI, Basel, Switzerland. This article is an open access article distributed under the terms and conditions of the Creative Commons Attribution (CC BY) license (<http://creativecommons.org/licenses/by/4.0/>).